**Atmospheric
Chemistry
and Physics
Discussions**

**Rates of cloud
droplet formation**

C. R. Ruehl et al.

Title Page	
Abstract	Introduction
Conclusions	References
Tables	Figures
◄◄	►►
◄	►
Back	Close
Full Screen / Esc	

Printer-friendly Version

Interactive Discussion

EGU

How quickly do cloud droplets form on atmospheric particles?

C. R. Ruehl[1], P. Y. Chuang[1], and A. Nenes[2,3]

[1]Earth & Planetary Sciences, University of California, Santa Cruz, California, USA
[2]Earth & Atmospheric Sciences, Georgia Institute of Technology, Atlanta, Georgia, USA
[3]Chemical and Biomolecular Engineering, Georgia Inst. of Technology, Atlanta, Georgia, USA

Correspondence to: C. R. Ruehl (cruehl@ucsc.edu)

Abstract

The influence of aerosols on cloud properties is an important modulator of the climate system. Traditional Köhler theory predicts the equilibrium concentration of cloud condensation nuclei (CCN); however, it is not known to what extent particles exist in the atmosphere that may be prevented from acting as CCN by kinetic limitations. We measured the rate of cloud droplet formation on atmospheric particles sampled at four sites across the United States during the summer of 2006: Great Smoky Mountain National Park, TN; Bondville, IL; Houston, TX; and the Atmospheric Radiation Measurement Program Southern Great Plains site near Lamont, OK. We express droplet growth rates with the mass accommodation coefficient (α), and report values of α measured in the field normalized to the mean α measured for lab-generated ammonium sulfate (AS) particles (i.e., $\alpha'=\alpha/\alpha_{AS}$). Overall, 61% of ambient CCN grew at a rate similar to AS. We report the fraction of CCN that were "low-α'" ($\alpha'<10^{-0.33}$). Of the 16 days during which these measurements were made, 7 had relatively few low-α' CCN (<16%), 7 had moderate low-α' fractions (31% to 62%), and 2 had large low-α' fractions (>77% during at least one ~30 min period). Day to day variability was greatest in Tennessee and Illinois, and low-α' CCN were most prevalent on days when back trajectories suggested that air was arriving from aloft. The highest fractions of low-α' CCN in Houston and Illinois occurred around local noon, and decreased later in the day. These results suggest that for some air masses, accurate quantification of CCN concentrations may need to account for kinetic limitations.

1 Introduction

After several decades of research attempting to quantify the influence of human activities on the Earth's climate, the largest single source of uncertainty in the total anthropogenic radiative forcing of the atmosphere remains the effect of atmospheric particles on cloud properties, i.e., the indirect aerosol effects on climate (IPCC, 2007). The

ability to predict the size distribution of cloud droplets given an initial size distribution of suspended particles is essential if aerosol indirect effects are to be quantified. In the atmosphere, cloud droplets form on pre-existing aerosol particles, which can act as cloud condensation nuclei (CCN) when the ambient partial pressure of water vapor (p_w) exceeds the saturation vapor pressure (p_w^0) resulting in a supersaturation (S)

$$S = \frac{p_w}{p_w^0} - 1. \tag{1}$$

For almost a century, Köhler theory (Köhler, 1936) has been used to determine the minimum, or critical, supersaturation (S_c) required to activate a particle of known size and composition, causing the particle to grow into a cloud droplet via condensation of water vapor. More recently, modifications of Köhler theory have been proposed to incorporate various chemical effects, including slightly-soluble compounds (Shulman et al., 1996; Shantz et al., 2003), soluble gases (Kumala et al., 1993), surface tension reduction (Shulman et al., 1996; Facchini et al., 1999), and film-forming compounds (Feingold and Chuang, 2002). Adiabatic cloud parcel modeling suggests that the influence of these effects on cloud droplet concentration (N_d) is comparable to the influence of total particle concentration (Nenes et al., 2002).

Classical Köhler theory, however, predicts only the equilibrium S_c of a particle, and thus does not incorporate any potential kinetic limitations to cloud droplet formation. Chuang et al. (1997) pointed out that failure to take into account kinetic limitations could result in errors in calculated radiative forcing similar to that corresponding to current anthropogenic greenhouse gas concentrations ($\sim 2\,\text{W/m}^2$). It is therefore of interest if particles exist in the atmosphere that, under typical atmospheric supersaturations (~ 0.1 to 1%), would form cloud droplets at equilibrium, but cannot do so within realistic time scales (tens of seconds to a few minutes). These kinetic limitations could result from, for example, films at the droplet surface that limit transfer of water to the drop during condensation, or from slow dissolution of particulate matter. The kinetics of condensational growth are often represented by the mass accommodation coefficient (α), which conceptually is the probability that a water vapor molecule colliding with a

Rates of cloud droplet formation

C. R. Ruehl et al.

Printer-friendly Version

Interactive Discussion

EGU

[EGU](#)

droplet will be incorporated into the liquid phase. Although α for pure water droplets is expected to be ~1 (Laaksonenen, 2005), it is not known to what extent the atmosphere contains CCN whose growth rates during activation would be better fit using standard condensational growth theory with α less than 1. A great number of studies have concluded that the presence of an organic film at the aqueous-air interface can reduce α during condensation and/or evaporation to ~10^{-4} (e.g., Rubel and Gentry, 1984; Seaver et al., 1992). Cantrell et al. (2001) found that setting α equal to 10^{-4} produced the best fit between modelled and measured CCN concentrations near the Indian Ocean during a time when aerosol concentrations and organic fractions were relatively high. Chuang (2003) found that 0 to 2% of particles in Mexico City exhibited subsaturated condensational (i.e., hygroscopic) growth at a rate corresponding to α ~1 to 4×10^{-4}, but did not measure growth rates under supersaturated (i.e., droplet activating) conditions. Recently, Stroud et al. (2007) found that setting α equal to 0.07 produced the best fit between modeled growth and that observed for CCN sampled from a forest in the southeastern United States. In this study, we determine α for each observed activated droplet at realistic S values (0.13 to 0.63%), and thus determine the α distribution of atmospheric CCN.

Köhler theory can be tested by CCN closure experiments, in which CCN concentration predicted given particle size distribution and composition is compared to observations in a CCN instrument in which S is known. Closure experiments have been conducted in various settings, including near the Canary Islands, Spain (Snider and Brenguier, 2000; Chuang et al., 2000), the Southern Ocean (Covert et al., 1998), the Arctic Ocean (Zhou et al., 2001), the Indian Ocean (Cantrell et al., 2001), Amazonia (Rissler et al., 2004), Florida (VanReken et al., 2003), Nova Scotia (Ervens et al., 2007), New Hampshire (Medina et al., 2007), and North Carolina (Stroud et al., 2007). A smaller number of studies have compared predicted and observed in-situ cloud droplet concentrations (e.g., Hallberg et al., 1997; Snider et al., 2003; Conant et al., 2004). Although closure is often achieved within experimental uncertainties, when it is not achieved it is almost invariably due to overprediction of CCN concentrations. Often

discrepancies between predictions and observations can only be reduced by assuming that the aerosol soluble fraction is unrealistically low (e.g., Snider and Brenguier, 2000), or alternatively that all aerosol organic matter is insoluble (e.g., Cantrell et al., 2001), despite observations that some organic aerosol is CCN active (e.g., Novakov
5 and Penner, 1993). These discrepancies could be due to kinetic limitations to droplet growth, a possibility that seems more likely considering that most identified chemical effects on droplet activation lower S_c (e.g., surface tension reduction and dissolution of gases). If kinetic limitations to cloud droplet formation are important in the atmosphere, not only cloud properties but also the lifetime of aerosol particles and consequently
10 aerosol composition could be influenced. The purpose of this study was to measure α distributions for various ambient aerosols (urban, regional polluted, and background) to determine the extent to which potential kinetic limitations to droplet formation exist in the atmosphere.

2   Experimental

15 2.1   Site descriptions

All equipment was housed in a trailer, which was deployed at four sites across the United States during August–September 2006 (Fig. 1). The sites were selected to sample a variety of general air mass types: urban (HOU – Houston, TX), polluted regional (GSM – Great Smoky Mountain National Park, TN), and background continental
20 (BON – Bondville, IL, and SGP – the Southern Great Plains site, run by the U.S. Department of Energy Atmospheric Radiation Measurement program, near Lamont, OK). In Houston, particles were sampled on top of Moody Towers on the campus of the University of Houston, as part of the second Texas Air Quality Study (TexAQS II). Moody Towers is approximately 6 km southeast of downtown Houston, and 5 km southwest of
25 the Houston Ship Channel. $PM_{2.5}$ in the region is dominated by sulfate (32% by mass), organic carbon (30%), and ammonium (9%), and annual mean $PM_{2.5}$ concentrations

are 10 to 14 μg/m^3, with maximum hourly concentrations often $>$40 μg/m^3 (Russell et al., 2004). The GSM site was located at Look Rock, a long-term atmospheric monitoring station on a ridge along the western edge of the National Park. To the north and west of this ridge is a valley that includes the cities of Knoxville (36 km north) and Chattanooga (140 km southwest), as well as several interstate highways and coal-fired power plants. During the summer of 2001, the average PM$_{2.5}$ concentration at Look Rock was 19.0 μg/m^3, which by mass was 41% sulfate, 29% organic carbon, and 9% ammonium (Tanner et al., 2004). The BON site was at the Bondville Environmental and Atmospheric Research Site, maintained by the Illinois State Water Survey, 14 km southwest of Urbana-Champaign. Throughout a field campaign conducted at BON from March 2001 to May 2003, the average PM$_{2.5}$ concentration was 9.5 μg/m^3, of which (by mass) 12% was organic carbon, 28% was sulfate, and 17% was nitrate (Kim et al., 2005). The Southern Great Plains (SGP) site, located 38 km southwest of Ponca City, OK, is maintained by the U.S. Department of Energy's Atmospheric Radiation Measurement Program. Summer submicron aerosol at the site from 1997 through 2001 was dominated by sulfate and ammonium (23 to 30% and 9 to 12% by mass, respectively), and concentrations averaged 12.1 μg/m^3 (organic carbon was not quantified) (Iziomon and Lohmann, 2003).

2.2 Instrumentation

Condensational growth rates were measured for both generated ammonium sulfate particles, used as reference particles, and ambient particles sampled in the field. This was accomplished by exposing particles to a water vapor supersaturation (i.e., $S>0$) for a known duration in a supersaturating column (SSC), and then measuring the resulting droplet size with a phase doppler interferometer (PDI). The SSC produces a water vapor supersaturation along its centerline when an increasing temperature gradient (ΔT) is applied to its walls (Fig. 2). Both S and the duration of the exposure can be controlled by adjusting the SSC flow rate and ΔT. This technique is identical to

Rates of cloud droplet formation

C. R. Ruehl et al.

Title Page

Abstract | Introduction

Conclusions | References

Tables | Figures

◄ | ►

◄ | ►

Back | Close

Full Screen / Esc

Printer-friendly Version

Interactive Discussion

EGU

EGU

the continuous-flow streamwise thermal-gradient cloud condensation nuclei chamber described in Roberts and Nenes (2005). Particles were initially passed through a humidity conditioner that maintained the relative humidity (RH) at ~80%. The particles were then sent to a differential mobility analyzer (DMA). The DMA selected a quasi-monodisperse particle population with a mean diameter in the range of 100 to 250 nm. This flow was then divided between a condensation nucleus counter (CNC, TSI 3010) and the SSC-PDI. After flowing for 10 s through an isothermal entrance length with RH ~100%, particles were exposed to a known S in the SSC for 30 s. The velocity and diameter (D) of the activated droplets was then measured with the PDI while still subject to S (i.e., before the particles exited the SSC).

Along the centerline of the SSC, the calibrated value of S at any given ΔT is determined by the mobility diameter of lab-generated AS particles selected by the DMA at which half are activated. Under the DMA conditions used for this calibration, the geometric standard deviation of the DMA transfer function is approximately 1.05, which corresponds to an absolute uncertainty in S_c of 0.01% at the low end of the calibration (0.11%) and 0.04% at the high end (0.63%). Temperature fluctuations in the SSC were monitored with thermistors and were typically ~0.01 K, which would produce a negligible uncertainty in S relative to the uncertainty associated with the DMA transfer function. Likewise, SSC flow rate fluctuations are expected to be minimal, as this flow passed through a critical orifice immediately downstream of the column. However, there were at times substantial variations in the droplet velocity measured by the PDI, possibly due to deviations from a parabolic velocity profile in the SSC. We therefore omitted any measurements in which the PDI velocity was more than 5% higher or lower than that predicted for parabolic flow. These were typically <20% of all measurements, and tended to occur immediately after changing the temperature gradient in the column, and/or when ΔT was relatively high (~20 K/m). The resulting uncertainty in droplet size due to velocity fluctuations is minimized, however, because when the droplet velocity is greater, the S experienced for a given ΔT increases (enhancing droplet growth), whereas the residence time in the SSC decreases (inhibiting droplet

growth). Therefore, uncertainty in droplet growth rate based on measurements of D are expected to be less than those associated with the <5% deviation from parabolic flow velocity discussed above.

There are several advantages to using a phase Doppler interferometer to measure droplet diameter. Conventional light-scattering probes direct a single laser beam into a stream of particles, which scatter light when they intersect the beam. The diameter is determined by the intensity of the scattered light signal. A PDI, on the other hand, consists of two laser beams that form a view volume at their intersection (Sankar et al., 1991; Bachalo and Sankar, 1996), which in this system is on the centerline of the SSC. When droplets pass through this view volume, three photodetectors aligned along the axis of the SSC measure this signal. The phase differences between the photodetector signals are determined by the optical divergence of the droplet, which is a function of D. Therefore the D measurement depends only on these phase differences, and is independent of signal intensity. This is an advantage because signal intensity can be influenced by detector response, laser strength, and absorption/scattering of light by condensation on SSC walls or smaller droplets off the SSC centerline, all of which can vary with time. We therefore were able to place the view volume in the SSC while the droplets were still exposed to S by aligning the beams and photodetectors with windows that were built into the SSC, and any minor condensation on the windows did not influence diameter measurements. The PDI probe used in these experiments can detect droplets with $D{\geq}0.5\,\mu\mathrm{m}$, with an accuracy of $\pm0.5\,\mu\mathrm{m}$. We assume that the droplets were still exposed to the average centerline S when they passed through the view volume even though the temperature gradient ended ${\sim}2\,\mathrm{cm}$ above the windows. This is because water vapor and heat diffusing from the inner wall of the SSC to the centerline are also carried downwards by the flow in the SSC. Droplets in the view volume experience a water vapor pressure equal to that along the wall some distance above the view volume. This distance (x) is roughly equal to the ratio of the average velocity inside the SSC ($\bar{v}_{\mathrm{SSC}}$) to the timescale of water vapor diffusion (τ_w) (Roberts

and Nenes, 2005)

$$x = \bar{v}_{SSC}\tau_w = \frac{\bar{v}_{SSC}R_{SSC}^2}{D_v} \tag{2}$$

where R_{SSC} is the inner radius of the SSC (0.011 m) and D_v is the diffusivity of water vapor in air (2.5×10^{-5} m^2/s at 298 K and 1 atm). All results presented here are for $\bar{v}_{SSC}$=0.011 m/s, which when used in Eq. (2) results in x>5 cm, suggesting that the droplets in the view volume are still experiencing the characteristic S of the SSC. Additionally, the PDI ensures that only droplets along the SSC centerline are measured (the view volume dimensions are less than 1 mm perpendicular to the direction of sample flow), i.e., droplets are exposed to a single (maximum) S. Finally, as discussed above, the PDI also determines droplet velocity based on the frequency of the scattered light signal, and thus we were able to verify that parabolic flow had developed in the SSC and consequently to minimize uncertainty in the SSC residence time.

2.3 SSC model

We represent droplet growth rates by transforming observed drop size distributions into α distributions with a fully-coupled numerical flow model that simulates conditions in the SSC (Roberts and Nenes, 2005). This model calculates the final D given initial particle composition and size, α, ΔT (which determines S, based on calibration with dry ammonium sulfate particles) and flow rate (i.e., duration of exposure to S). The model solves the time-dependent equations for droplet condensational growth in a water vapor supersaturation (Fukuta and Walter, 1970)

$$D\frac{dD}{dt} = \frac{S - S_{eq}}{\frac{\rho_w RT}{4p_w^0 D_v' M_w} + \frac{\rho_w M_w \Delta H_v}{4k'T}\left(\frac{\Delta H_v}{RT} - 1\right)} \tag{3}$$

where S_{eq} is the equilibrium supersaturation of the particle (i.e., the solution to the Köhler equation), ρ_w, M_w, and ΔH_v are the density, molecular mass, and molar heat

14241

EGU

of vaporization of water, R is the gas constant, T is the temperature, and D'_v and k' are the diffusivity and thermal conductivity of water vapor corrected for noncontinuum effects. The size of this correction for D'_v depends on α (Fukuta and Walter, 1970)

$$D'_v = \frac{D_v}{1 + \frac{2D_v}{\alpha D}\sqrt{\frac{2\pi M_w}{RT}}}. \tag{4}$$

5 Although we are able to measure droplet growth rates, we are not able to determine the mechanism causing some droplets to grow more slowly than others. If kinetic limitations are caused by slow dissolution, or diffusion of solute to the droplet-air interface, droplet growth will be limited by the Raoult Effect (i.e., the lowering of liquid water activity due to the presence of solute). These mechanisms would increase S_{eq} in Eq. (2),
10 leading to a reduction in the difference in water activity between the droplet and its surroundings that drives condensational growth (S-S_{eq}), as opposed to a true reduction in mass accommodation. Because the mechanism causing any changes in growth rate is unknown, we refer to the *apparent* mass accommodation coefficient (α_{app}) when representing droplet growth rates.

15 Because the composition of particles in the field is unknown, there is no way to know a priori what their critical supersaturations (S_c) are. However, when the duration of exposure to S is 30 s and S is relatively high, the modeled α_{app} is relatively insensitive to S_c. For example, when condensation occurs on AS particles with D_{dry}=100 nm for 30 s, the minimum diameter detectable by the PDI, $\sim$0.5 μm, corresponds to α_{app}=$10^{-3.5}$
20 (Fig. 3a). When the particles are assumed to be composed of 5% AS and 95% insoluble material, S_c increases from $\sim$0.12% to $\sim$0.30%, but at higher S, droplets with α_{app} $\sim$$10^{-3}$ are still detectable by the PDI (Fig. 3b). The difference between these two cases, i.e., the error in α_{app} introduced when assuming a 5% soluble particle is fully soluble (Fig. 3c), is small (<0.2 in log space) when S is at least 0.1% larger than S_c
25 for activating droplets. This is because after activation, S_{eq} drops from S_c to $\sim$ 0 as the droplet grows, and therefore, as can be seen in Eq. (3), the rate of droplet growth

Rates of cloud droplet formation

C. R. Ruehl et al.

Title Page

Abstract	Introduction
Conclusions	References
Tables	Figures

◄◄   ►►

◄   ►

Back   Close

Full Screen / Esc

Printer-friendly Version

Interactive Discussion

EGU

depends primarily on S, which is known, and α. It has been previously noted that the hygroscopicity of internally mixed (soluble/insoluble) aerosols is dominated by the soluble fraction, even in small proportions (Bilde and Svenningsson, 2004). We therefore use AS particles with D_{dry}=100 nm in the model, and assume that meaningful values of α_{app} will be derived as long as ambient particles with D (at RH ~80%) from 100 to 250 nm are sampled, and measurements are made at several values of S. Because the hygroscopic and CCN properties of AS are relatively well known, we use it as a reference compound, and therefore all field measurements of α_{app} are reported normalized to those of lab-generated AS particles with D=100 nm (at RH ~80%)

$$\alpha' = \frac{\alpha_{app}}{\alpha_{app,AS}}. \tag{5}$$

3 Results

3.1 Lab measurements of α_{app}

Ammonium sulfate (AS) particles were generated in the lab and sent through the same RH conditioner used in the field (producing an RH ~80%) before size-selection by the DMA. α_{app} of these particles was determined from PDI measurements of D, and did not vary significantly when initial wet particle D was changed from 100 nm to 250 nm. Over S ranging from 0.18% to 0.43% (roughly corresponding to the range of D detectable by PDI), $\alpha_{app,AS}$, was $10^{-2.03\pm0.16}$ (Fig. 4). The uncertainty of a factor of $10^{0.16}$ quoted is 1σ. Therefore, according to Eq. (5), we report all field measurements of α_{app} normalized to AS as $\alpha'=10^{2.0}\times\alpha_{app}$. Furthermore, because they are significantly different from AS droplets (by at least 2σ), we refer to CCN with $\alpha'<10^{-0.33}$, $\alpha'<10^{-1}$, and $\alpha' >10^{0.33}$ as "low-α'," "very low-α'," and "high-α'" CCN, respectively, and report the fraction of CCN that were low-α' (f_L), very low-α' (f_{VL}), and high-α' (f_H).

Rates of cloud droplet formation

C. R. Ruehl et al.

EGU

3.2 Field measurements of α'

The growth rate of droplets was measured as described above on a total of 16 days between 10 August and 22 September, 2006 (See Table 1 for a summary of all measurements). On days when different time periods yielded distinct results, the periods are listed separately. Overall, α' for most droplets (61%) was between $10^{-0.33}$ and $10^{0.33}$ (i.e., α_{app} within 2σ of droplets formed on AS particles), but among the sites this fraction of CCN with similar growth rates to AS ranged from 45% at BON to 78% at GSM (Fig. 5). GSM was characterized by relatively large day-to-day variability in α' distributions, but was the only site where high-α' CCN were detected every day (Fig. 6). Daily variability in α' distributions was also relatively high at BON, which had the highest fraction of low-α' CCN (f_L =50%) among the sites (Fig. 7). HOU had less daily variability than GSM and BON, and the second-highest f_L (44%) (Fig. 8). Less data was available from SGP than the other sites, but CCN from this site did have similar growth kinetics to those from HOU, although no high-α' CCN were detected (Fig. 9). For individual time periods at all sites, f_L and f_{VL} ranged from 0 to 94% and 0 to 21%, respectively, and f_H ranged from 0 to 67%.

Among the 16 days, we identify those with either (a) little/no, (b) moderate, or (c) strong kinetic inhibition to condensational growth, as well as those with (d) kinetic enhancement to growth (see Table 1). Seven of the 16 days had little/no inhibition (f_{VL} <0.9% and f_L<16%), 7 days had at least one period with moderate inhibition (f_{VL} <3.2% and 31%< f_L <62%), and 2 days had at least one period with strong inhibition (f_{VL}> 8.4% and f_L> 77%). Also, we detected CCN with enhanced kinetic growth (2.8%<f_H<67%) on 11 out of 16 days. All 4 sites experienced at least one day with moderate or strong inhibition to condensational growth relative to AS, including both days at SGP and 4 out of 5 days at HOU, although relatively few very low-α' CCN (f_{VL} =0.6%) were detected at SGP. Moderate inhibition was observed on one out of 4 days at the polluted regional site (GSM), and 2 out of 5 days at one of the continental background site (BON) had strong inhibition to growth. On both days with strong

inhibition, kinetic limitations peaked around local noon and decreased later in the day (Fig. 10). A decrease in low-α' CCN later in the day was also seen at HOU (Fig. 11). Kinetic enhancement to condensational growth (relative to AS) was also observed, but typically in a much smaller fraction of CCN than those with inhibited growth. The pol-
luted regional site (GSM) had the highest amount of high-α' CCN (f_H=7.2%), followed by BON (4.9%), HOU (3.8%), and SGP (0).

4 Discussion/conclusions

To potentially explain the observed daily variability in droplet growth rates, we compared back trajectories for the days during which measurements were taken at BON and GSM (Figs. 12 and 13, respectively). According to these analyses, air masses descending from > 1000 m elevation arrived both days at BON that had highest-observed low-α' CCN (Figs. 12b, c), but were absent on other days (Figs. 12a, d). A similar pattern was seen at GSM: air from aloft (>1000 m elevation) was arriving throughout the one day in which there was moderate inhibition to condensational growth (Fig. 13c), whereas on other days descending air was either absent or intermittent (Figs. 13a, b, d). If air arriving from aloft contains accumulation mode aerosols that have survived one or more cloud cycles, and these cycles selectively remove high-α' CCN via wet deposition, low-α' CCN should be more prevalent. Novakov et al. (1997) observed an increase in aerosol carbon mass fraction with altitude in the eastern United States. Similarly, Andrews et al. (2004) observed a slight decrease in single-scatter albedo with altitude above SGP in data collected over two years, which was likely due to an increase in carbonaceous content. Other studies have confirmed the abundance of organic matter aerosols in the free troposphere (e.g., Murphy et al., 1998; Heald et al., 2005). Most potential mechanisms of kinetic limitations to droplet growth likely involve organic matter (e.g., slowly-dissolving or film-forming compounds), and therefore the preponderance of organic material in free tropospheric aerosols is consistent with our observations that low-α' CCN seemed to be more prevalent in air masses arriving from

EGU

aloft.

Kinetic inhibitions to condensational growth were strong on two days at BON, and although there was less daily variability at HOU, one period during 7 September had more low-α' (f_L =62%) than all other HOU times (f_L <48%). On each of these three days, kinetic limitations peaked around noon, and decreased later in the day. It is possible that photochemical aging of the ambient aerosol on those days caused the particles to become more oxidized and therefore more soluble, and that this is the reason for the consistent decrease in low-α' droplets throughout the afternoon. Much more data would be required, however, to rigorously test this hypothesis. We also observed CCN that grew more rapidly than lab-generated AS. One possible explanation for this is the presence of surface-active substances that might act to lower S_{eq}, and thus increase the difference between S and S_{eq} that drives condensational growth, i.e., the numerator on the right side of Eq. (3). Again, more data would be required, including compositional data, before this mechanism for increased growth rates could be verified.

These results suggest that aerosols containing CCN with α_{app} significantly lower than that observed for laboratory-generated AS are fairly common in the atmosphere, as they were observed on nine out of sixteen days at four different field sites. Kinetic limitations of this magnitude could keep these particles from being activated under atmospherically relevant timescales of exposure to water vapor supersaturation (i.e., ~30 s). These particles could be partly responsible for overprediction of CCN concentrations in previous closure experiments, and could also lead to broadening of cloud droplet spectra that might diminish the affect of increased aerosol concentrations on cloud radiative properties (Liu and Daum, 2002). Low-α' CCN might also have a longer atmospheric lifetime than other particles due to less efficient removal by wet deposition. Less efficient removal could, in fact, explain why slowly-growing particles seemed to be present in air masses arriving from aloft, if a portion of the particles in these masses had already been subject to one or more cloud cycles.

EGU

References

10 Andrews, E., Sheridan, P. J., Ogren, J. A., and Ferrare, F.: In situ aerosol profiles over the Southern Great Plains cloud and radiation test bed site: 1. Aerosol optical properties, J. Geophys. Res., 109, D06208, doi:10.1029/2003JD004025, 2004.

Bachalo, W. D. and Sankar, S. V.: Phase Doppler particle analyzer, in: Handbook of Fluid Dynamics, edited by: Johnson, R. W., CRC Press, 1996.

15 Bilde, M. and Svenningsson, B.: CCN activation of slightly soluble organics: the importance of small amounts of inorganic salt and particle phase, Tellus B, 128–134, 2004.

Cantrell, W., Shaw, G., Cass, G. R., Chowdhury, Z., Hughes, L. S., Prather, K. A., Guazzotti, S. A., and Coffee, K. R.: Closure between aerosol particles and cloud condensation nuclei at Kaashidhoo Climate Observatory, J. Geophys. Res., 106, 28 711–28 718, 2001.

20 Chuang, P. Y., Charlson, R. J., and Seinfeld, J. H.: Kinetic limitations on droplet formation in clouds. Nature, 390, 594–596, 1997.

Chuang, P. Y., Collins, D. R., Pawlowska, H., Snider, J. R., Jonsson, H. H., Brenguier, J.-L., Flagan, R. C., and Seinfeld, J. H.: CCN measurements during ACE-2 and their relationship to cloud microphysical properties, Tellus, 52B, 843–867, 2000.

25 Chuang, P. Y.: Measurement of the timescale of hygroscopic growth for atmospheric aerosols, J. Geophys. Res., 108, 4282, doi:10.1029/2002JD002757, 2003.

Conant, W. C., VanReken, T. M., Rissman, T. A., Varutbangkul, V., Jonsson, H. H., Nenes, A., Jimenez, J. L., Delia, A. E., Bahreini, R. Roberts, G. C., Flagan, R. C., and Seinfeld, J. H.: Aerosol–cloud drop concentration closure in warm cumulus. J. Geophys. Res., 109, D13204,
30 doi:10.1029/2003JD004324, 2004.

Rates of cloud droplet formation

C. R. Ruehl et al.

Covert, D. S., Gras, J. L., Wiedensohler, A., and Stratmann, F.: Comparison of directly measured CCN with CCN modeled from the number-size distribution in the marine boundary layer during ACE 1 at Cape Grim, Tasmania, J. Geophys. Res., 103, 16 597–16 608, 1998.

Ervens, B., Cubison, M., Andrews, E., Feingold, G., Ogren, J. A., Jimenez, J. L., DeCarlo, P., and Nenes, A.: Prediction of cloud condensation nucleus number concentration using measurements of aerosol size distributions and composition and light scattering enhancement due to humidity, J. Geophys. Res., 112, D10S32, doi:10.1029/2006JD007426, 2007.

Facchini, M. C., Mircea, M., Fuzzi, S., and Charlson, R. J.: Cloud albedo enhancement by surface-active organic solutes in growing droplets, Nature, 401, 257–259, 1999.

Feingold, G. and Chuang, P. Y.: Analysis of the influence of film-forming compounds on droplet growth: Implications for cloud microphysical processes and climate, J. Atmos. Sci., 59, 2006–2018, 2002.

Hallberg, A., Wobrock, W., Flossmann, A. I., Bower, K. N., Noone, K. J., Wiedensohler, A., Hansson, H.-C., Wendisch, M., Berner, A., Kruisz, C., Laj, P., Facchini, M. C., Fuzzi, S., and Arends, B. G.: Microphysics of clouds: Model vs. measurements. Atmos. Environ., 31, 2453–2310, 1997.

Heald, C. L., Jacob, D. J., Park, R. J., Russell, L. M., Huebert, B. J., Seinfeld, J. H., Liao, H., and Weber, R. J.: A large organic aerosol source in the free troposphere missing from current models. Geophys. Res. Lett., 32, L18809, doi:10.1029/2005GL023831, 2005.

IPCC: Contribution of Working Group I to the Fourth Assessment Report of the Intergovernmental Panel on Climate Change, Solomon, S. et al. (Eds.), Cambridge University Press, 2007.

Iziomon, M. G. and Lohmann, U.: Characteristics and direct radiative effect of mid-latitude continental aerosols: the ARM case, Atmos. Chem. Phys., 3, 1903–1917, 2003, http://www.atmos-chem-phys.net/3/1903/2003/.

Kim, E., Hopke, P. K., Kenski, D. M., and Koerber, M.: Sources of fine particles in a rural midwestern U.S. area, Environ. Sci. and Technol., 39, 4953–4960, 2005.

Köhler, H.: The nucleus in and the growth of hygroscopic droplets. T. Faraday Soc., 32, 1152–1161, 1936.

Kulmala, M., Laaksonen, A., Korhonen, P., Vesala, T., Ahonen, T., and Barrett, J.: The effect of atmospheric nitric acid vapor on cloud condensation nucleus activation, J. Geophys. Res., 98, 22 949–22 958, 1993.

Laaksonen, A., Vesala, T., Kulmala, M., Winkler, P. M., and Wagner, P. E.: Commentary on

EGU

cloud modelling and the mass accommodation coefficient of water, Atmos. Chem. Phys., 5, 461–464, 2005,
http://www.atmos-chem-phys.net/5/461/2005/.

Liu, Y. and Daum, P. H.: Anthopogenic aerosols: Indirect warming effect from dispersion forcing, Nature, 419, 580–581, 2002.

Medina, J., Nenes, A., Sotiropoulou, R.-E. P., Cottrell, L. D., Ziemba, L. D., Beckman, P. J., and Griffin, R. J.: Cloud condensation nuclei closure during the International Consortium for Atmospheric Research on Transport and Transformation 2004 campaign: Effects of size-resolved composition, J. Geophys. Res., 112, D10S31, doi:10.1029/2006JD007588, 2007.

Murphy, D. M., Thomson, D. S., and Mahoney, M. J.: In situ measurements of organics, meteoric material, mercury, and other elements in aerosols at 5 to 19 kilometers, Science, 282, 1664–1669, 1998.

Nenes, A., Charlson, R. J., Facchini, M. C., Kulmala, M., Laaksonen, A., and Seinfeld, J. H.: Can chemical effects on cloud droplet number rival the first indirect effect?, Geophys. Res. Lett., 29, 1848, doi:10.1029/2002GL015295, 2002.

Novakov, T. and Penner, J. E.: Large contribution of organic aerosols to cloud-condensation-nuclei concentrations, Nature, 365, 823–826, 1993.

Novakov, T., Hegg, D. A., and V. Hobbs, P. V.: Airborne measurements of carbonaceous aerosols on the East Coast of the United States, J. Geophys. Res., 102, 30 023–30 030, 1997.

Rissler, J., Swietlicki, E., Zhou, J., Roberts, G., Andreae, M. O., Gatti, L. V., and Artaxo, P.: Physical properties of the sub-micrometer aerosol over the Amazon rain forest during the wet-to-dry season transition – comparison of modeled and measured CCN concentrations, Atmos. Chem. Phys., 4, 2119–2143, 2004,
http://www.atmos-chem-phys.net/4/2119/2004/.

Roberts, G. C. and Nenes, A.: A continuous-flow streamwise thermal-gradient CCN chamber for atmospheric measurements, Aerosol Sci. Tech., 39, 206–221, 2005.

Rubel, G. O. and Gentry, J. W.: Measurement of the kinetics of solution droplets in the presence of adsorbed monolayers: Determination of water accommodation coefficients, J. Phys. Chem.-U.S., 88, 3142–3148, 1984.

Russell, M., Allen, D., Collins, D., and Fraser, M.: Daily, seasonal, and spatial trends in $PM_{2.5}$ mass and composition in southeast Texas. Aerosol Sci. Tech., 38, 14–26, 2004.

Sankar, S. V., Weber, B. J., Kamemoto, D. Y., and Bachalo, W. D.: Sizing fine particles with the

EGU

phase Doppler interferometric technique, Appl. Optics, 30, 4914–4920, 1991.

Seaver, M., Peele, J. R., Manuccia, T. J., Rubel, G. O., and Ritchie, G.: Evaporation kinetics of ventilated waterdrops coated with octadecanol monolayers. J. Phys. Chem.-U.S., 96, 6389–6394, 1992.

5 Shantz, N. C., Leaitch, W. R., and Caffrey, P. F.: Effect of organics of low solubility on the growth rate of cloud droplets, J. Geophys. Res., 108, 4168, doi:10.1029/2002JD002540, 2003.

Snider, J. R. and Brenguier, J.-L.: Cloud condensation nuclei and cloud droplet measurements during ACE-2, Tellus B, 828–842, 2000.

Snider, J. R., Guibert, S., Brenguier, J.-L., and Putaud, J.-P.: Aerosol activation in marine
10 stratocumulus clouds: 2. Köhler and parcel theory closure studies, J. Geophys. Res., 108, 8629, doi:10.1029/2002JD002692, 2003.

Stroud, C. A., Nenes, A., Jimenez, J. L., DeCarlo, P. F, Huffman, J. A., Bruintjes, R., Nemitz, E., Delia, A. E., Toohey, D. W., Guenther, A. B., and Nandi, S.: Cloud activating properties of aerosol observed during CELTIC, J. Atmos. Sci., 64, 441–459, 2007.

15 Tanner, R. L., Parkhurst, W. J., Valente, M. L., and Phillips, W. D.: Regional composition of $PM_{2.5}$ aerosols measured at urban, rural, and "background" sites in the Tennessee valley, Atmos. Environ., 38, 3143–3153, 2004.

VanReken, T. M., Rissman, T. A., Roberts, G. C., Varutbangkul, V., Jonsson, H. H., Flagan, R. C., and Seinfeld, J. H.: Toward aerosol/cloud condensation nuclei (CCN) closure during
20 CRYSTAL-FACE, J. Geophys. Res., 108, 4633, doi:10.1029/2003JD003582, 2003.

Zhou, J. C., Swietlicki, E., Berg, O. H., Aalto, P. P., Hameri, K., Nilsson, E. D., and Leck, C.: Hygroscopic properties of aerosol particles over the central Arctic Ocean during summer, J. Geophys. Res., 106, 32 111–32 123, 2001.

EGU

Table 1. Results of all Droplet Growth Rate Measurements.

date	local time	site	n	S range (%)	f_{VL} (%)	f_L (%)	f_H (%)
10 Aug 2006[a,d]	10:35–15:32	GSM	1867	0.29	0.7	16	7.8
12 Aug 2006[a,d]	12:12–19:02	GSM	481	0.24–0.31	0.1	9.1	2.8
13 Aug 2006[b,d]	12:58–15:22	GSM	101	0.18–0.31	3.2	31	16
15 Aug 2006[a,d]	21:27–21:32	GSM	19	0.47	0.0	5.1	11
GSM total		GSM	2468		0.7	15	7.2
19 Aug 2006[a]	13:58–14:10	BON	58	0.33	0.0	15	0.0
23 Aug 2006[a,d]	13:17–15:26	BON	33	0.22	0.0	13	6.7
24 Aug 2006[c]	12:24–13:02	BON	420	0.33–0.41	0.9	66	0.0
	13:06–13:47	BON	202	0.23–0.30	8.4	77	0.0
	17:02–17:29	BON	95	0.37–0.41	0.0	49	0.0
25 Aug 2006[c,d]	11:49–12:27	BON	219	0.41–0.52	1.0	39	0.0
	13:06–14:22	BON	166	0.23–0.34	21	94	0.0
	14:38–17:18	BON	485	0.13–0.52	0.3	32	5.7
28 Aug 2006[c,d]	13:40–14:33	BON	85	0.16–0.37	0.0	0.0	67
BON total		BON	1763		3.3	50	4.9
4 Sep 2006[b,d]	16:27–16:50	HOU	43	0.33-0.35	2.6	37	23
6 Sep 2006[b,d]	17:29-19:39	HOU	123	0.30–0.44	2.5	35	12
7 Sep 2006[b,d]	11:47–12:09	HOU	553	0.34–0.56	0.8	62	0.0
	16:58–17:40	HOU	274	0.35–0.49	1.9	29	5.1
8 Sep 2006[a]	11:24–11:32	HOU	164	0.63	0.0	6.6	0.0
11 Sep 2006[b,d]	12:23–21:17	HOU	466	0.28–0.63	1.5	48	5.1
HOU total		HOU	1623		1.3	44	3.8
16 Sep 2006[b]	16:01–16:36	SGP	97	0.34–0.63	0.9	49	0.0
22 Sep 2006[b]	14:39–14:57	SGP	43	0.41–0.63	0.0	32	0.0
SGP total		SGP	140		0.6	44	0.0
total (all sites)			5994		1.6	34	5.4

[a] Little/no kinetic inhibitions to condensational growth.

[b] Moderate kinetic inhibition.

[c] Strong kinetic inhibition.

[d] Kinetic enhancement to growth.

EGU
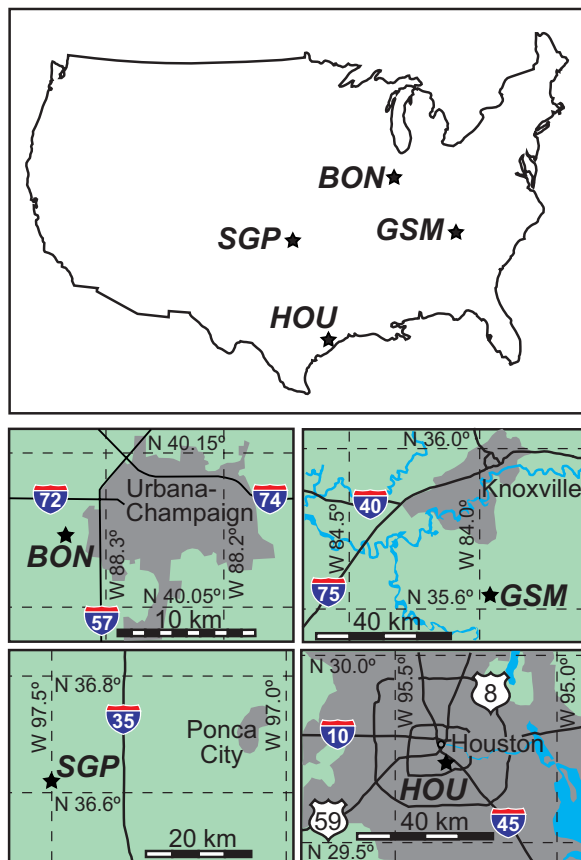
Fig. 1. United States map, showing locations of urban (HOU), polluted regional (GSM), and background continental (BON and SGP) sites, along with inset maps of each site.

Title Page

Abstract | Introduction

Conclusions | References

Tables | Figures

|◄ | ►|

◄ | ►
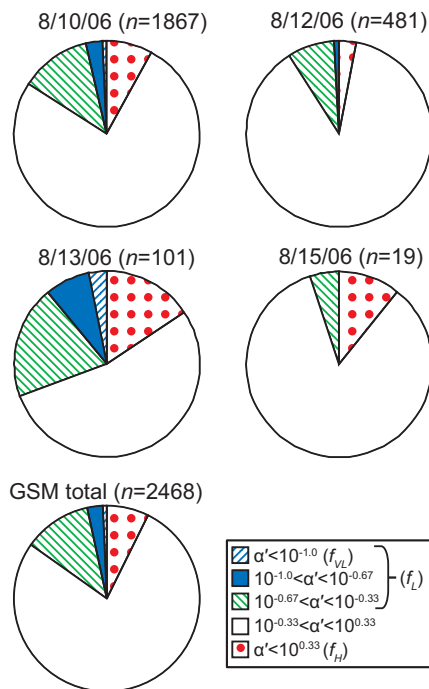
Back | Close

Full Screen / Esc

Printer-friendly Version

Interactive Discussion

EGU

EGU
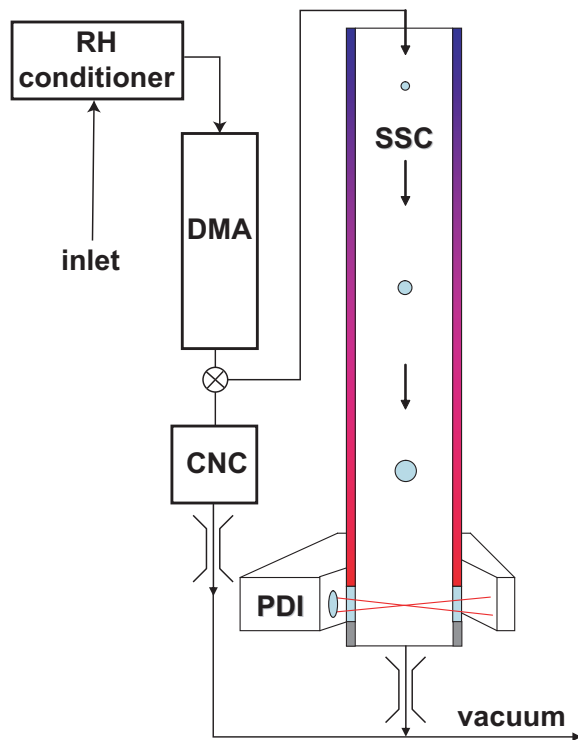
Fig. 2. Experimental schematic.

Printer-friendly Version

Interactive Discussion

EGU
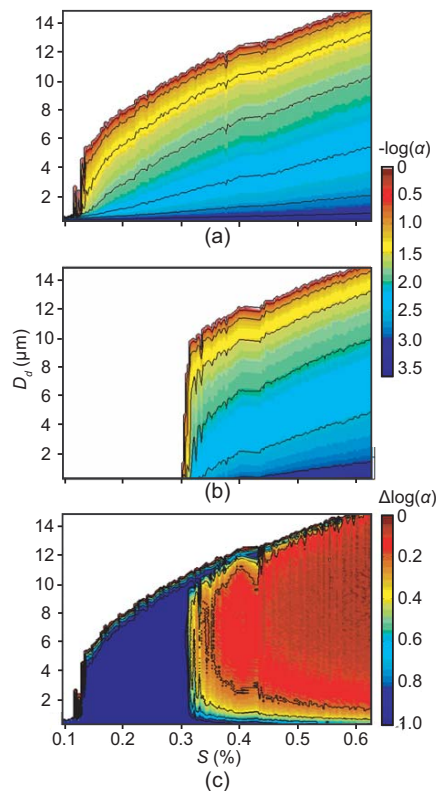
Fig. 3. (a) $\alpha(S,D)$ for 30 s of droplet growth on ammonium sulfate particles (100% soluble) with $D_{dry}=100$ nm. **(b)** Same as (a), but with 5% soluble particles. **(c)** Difference between (a) and (b).
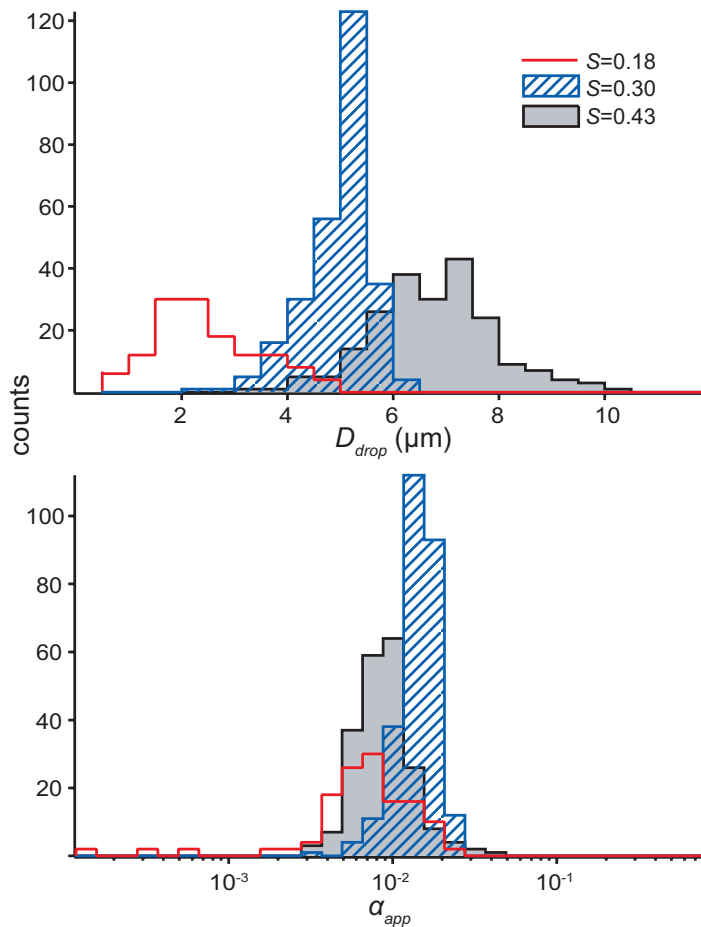
Fig. 4. D and α_{app} distributions after 30 s of condensational growth at 3 different supersaturations on lab-generated ammonium sulfate particles.

EGU

EGU
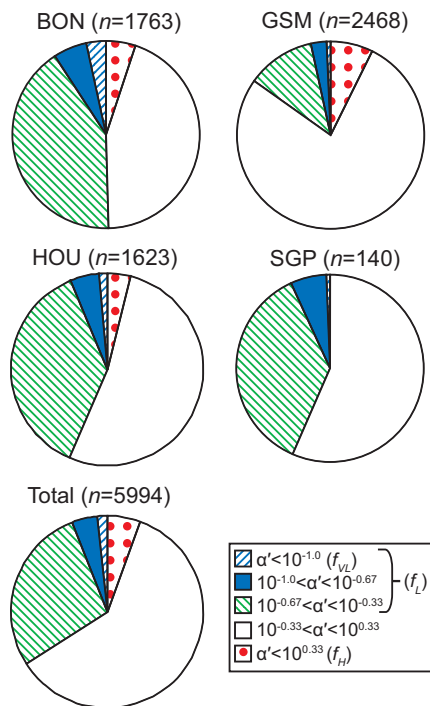
Fig. 5. Summary of CCN α' distributions at each site, and the total of all four sites. An α' of $10^{-1.0}$ is 6σ below the mean for ammonium sulfate ($\alpha_{app,AS}$), $\alpha'=10^{-0.67}$ is 4σ below $\alpha_{app,AS}$, $\alpha'=10^{-0.33}$ is 2σ below $\alpha_{app,AS}$, and $\alpha'=10^{0.33}$ is 2σ above $\alpha_{app,AS}$.

EGU

Fig. 6. Summary of CCN α' distributions for each day at GSM, and the total for the site. An α' of $10^{-1.0}$ is 6σ below the mean for ammonium sulfate ($\alpha_{app,AS}$), $\alpha'=10^{-0.67}$ is 4σ below $\alpha_{app,AS}$, $\alpha'=10^{-0.33}$ is 2σ below $\alpha_{app,AS}$, and $\alpha'=10^{0.33}$ is 2σ above $\alpha_{app,AS}$.

ACPD

7, 14233–14264, 2007

Rates of cloud droplet formation

C. R. Ruehl et al.

Title Page

Abstract | Introduction

Conclusions | References

Tables | Figures

|◄ | ►|

◄ | ►

Back | Close

Full Screen / Esc

Printer-friendly Version

Interactive Discussion

EGU
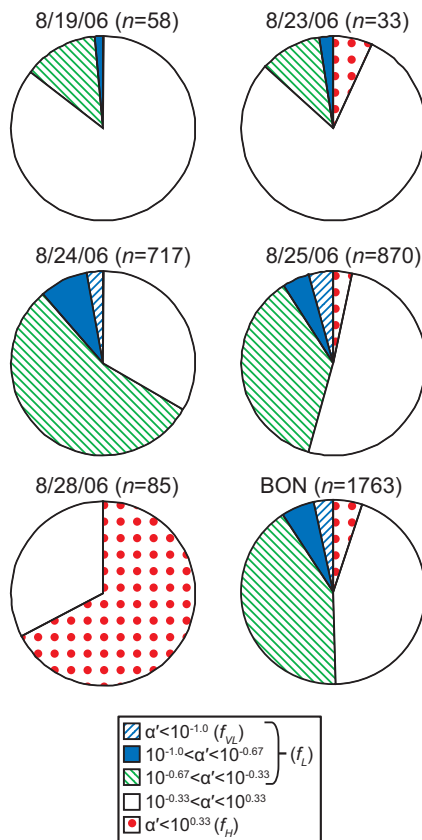
Fig. 7. Summary of CCN α' distributions for each day at BON, and the total from the site. An α' of $10^{-1.0}$ is 6σ below the mean for ammonium sulfate ($\alpha_{\mathrm{app,AS}}$), $\alpha'=10^{-0.67}$ is 4σ below $\alpha_{\mathrm{app,AS}}$, $\alpha'=10^{-0.33}$ is 2σ below $\alpha_{\mathrm{app,AS}}$, and $\alpha'=10^{0.33}$ is 2σ above $\alpha_{\mathrm{app,AS}}$.
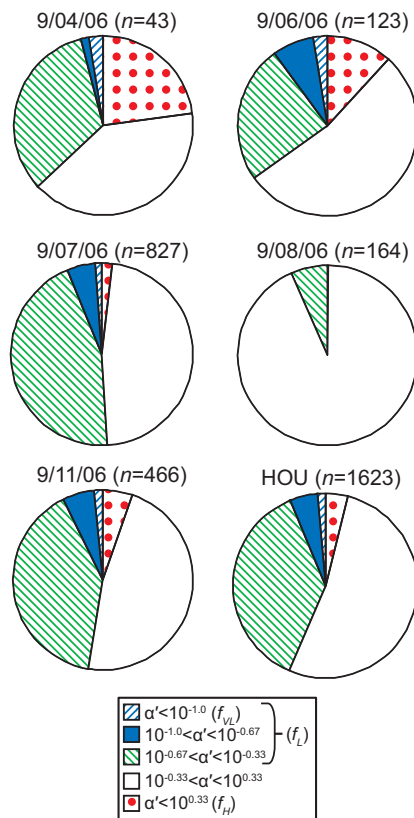
Fig. 8. Summary of CCN α' distributions for each day at HOU, and the total from the site. An α' of $10^{-1.0}$ is 6σ below the mean for ammonium sulfate ($\alpha_{app,AS}$), $\alpha'=10^{-0.67}$ is 4σ below $\alpha_{app,AS}$, $\alpha'=10^{-0.33}$ is 2σ below $\alpha_{app,AS}$, and $\alpha'=10^{0.33}$ is 2σ above $\alpha_{app,AS}$.

ACPD

7, 14233–14264, 2007

Rates of cloud droplet formation

C. R. Ruehl et al.

Title Page

Abstract | Introduction

Conclusions | References
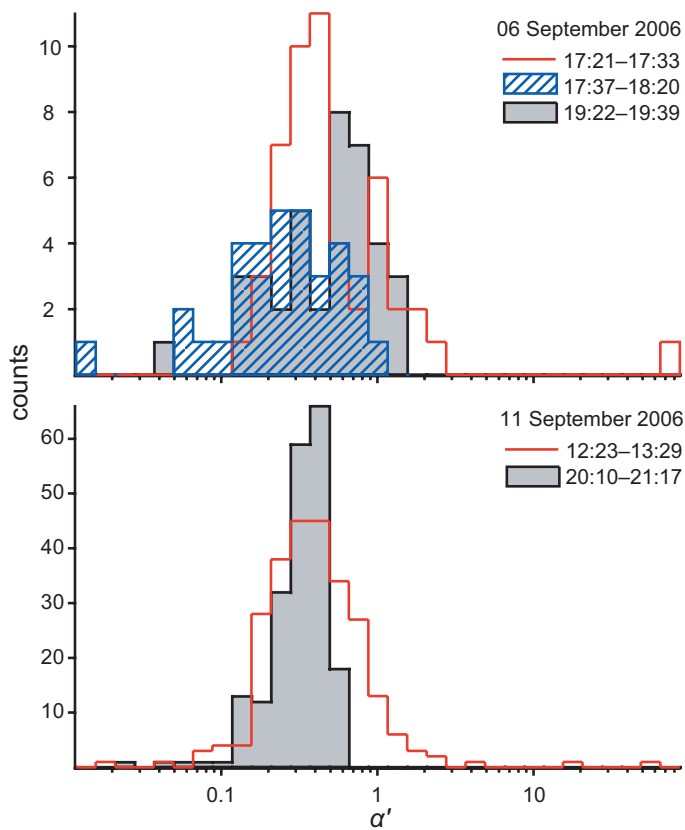
Tables | Figures

◀◀ | ▶▶

◀ | ▶

Back | Close

Full Screen / Esc

Printer-friendly Version

Interactive Discussion

EGU

EGU
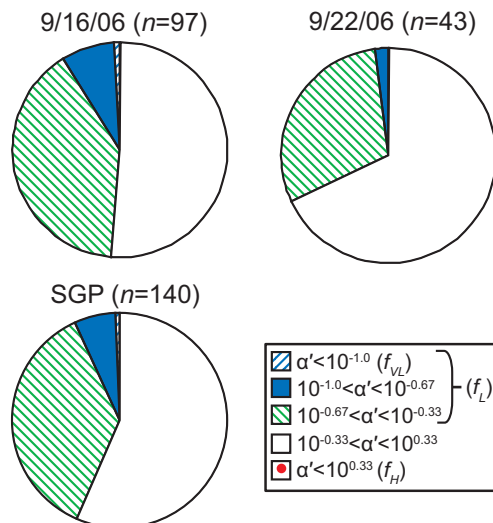
Fig. 9. Summary of CCN α' distributions for both days at SGP, and the total from the site. An α' of $10^{-1.0}$ is 6σ below the mean for ammonium sulfate ($\alpha_{app,AS}$), $\alpha'=10^{-0.67}$ is 4σ below $\alpha_{app,AS}$, $\alpha'=10^{-0.33}$ is 2σ below $\alpha_{app,AS}$, and $\alpha'=10^{0.33}$ is 2σ above $\alpha_{app,AS}$.
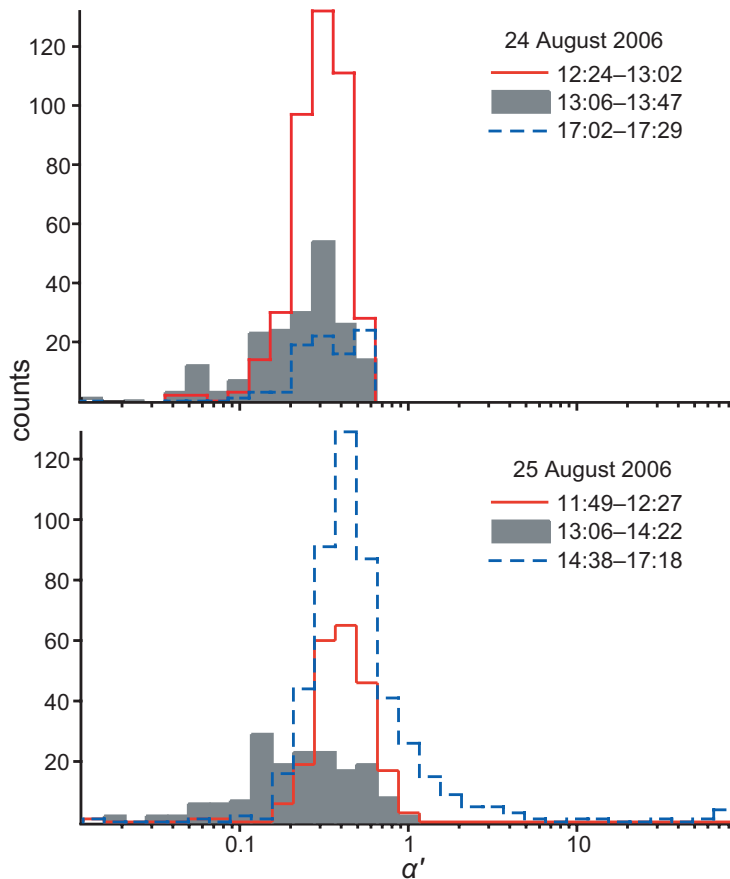
Fig. 10. α' distributions for various periods on the two days with strong inhibitions to condensational growth (both at BON).

EGU

Fig. 11. α' distributions for various periods on two days from HOU.

EGU
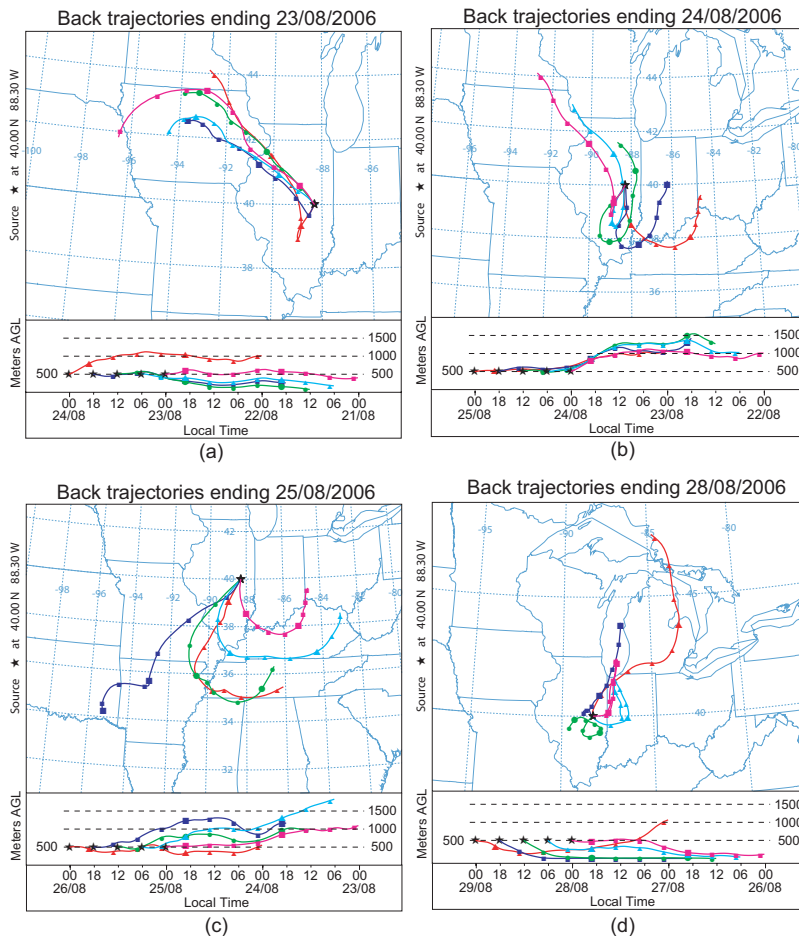
Fig. 12. NOAA HYSPLIT back trajectories ending at the BON site, ending on **(a)** 23 August 2006, **(b)** 24 August 2006, **(c)** 25 August 2006, and **(d)** 28 August 2006.

EGU
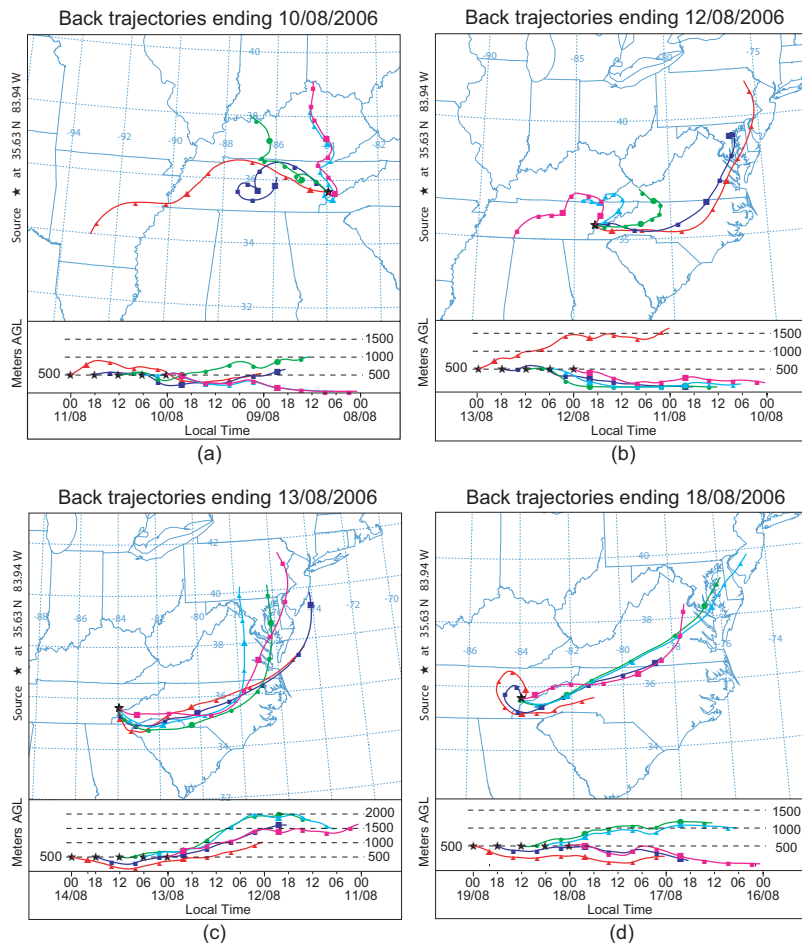
Fig. 13. NOAA HYSPLIT back trajectories ending at the GSM site, ending on **(a)** 10 August 2006, **(b)** 12 August 2006, **(c)** 13 August 2006, and **(d)** 18 August 2006.

EGU